Published in J. of Surveying Engineering, 18(1), 2022, https://doi.org/10.1061/(ASCE)SU.1943-5428.0000382

Precise orbit determination of LEO satellites based on undifferenced GNSS observations: a review

Amir Allahvirdi-Zadeh[1], Kan Wang[2], Ahmed El-Mowafy[3]

Abstract

Precise Orbit Determination (POD) is the procedure for determining the orbit of a satellite with high accuracy. Compared with Global Navigation Satellite Systems (GNSS), the Low Earth Orbit (LEO) satellites have some different features in space, mainly due to perturbations caused by dynamic forces related to their altitudes. Methods for POD of LEO satellites have been developed over the past decades. Nowadays, post-processed precise orbits are used in different space applications such as radio occultation, satellite altimetry, and interferometric synthetic-aperture radar missions. The advancements in technology decrease the size of LEO satellites and developments in theory increase their orbital accuracy. In recent years, onboard POD has become a hot topic in the navigation and positioning field, which is crucial for, e.g., formation-flying of small satellites and GNSS-aided LEO mega-constellations for positioning purposes. This contribution reviews LEO POD methods based on undifferenced GNSS observations in both post-mission and real-time data processing. It comprises the quality control step, the models used and their limitations, processing algorithms, and different validation methods. To have a clear insight into the current and the future state of the LEO POD, the most recent developments and important achievements are also discussed.

Keyword Precise Orbit Determination (POD) - Precise Point Positioning (PPP) - kinematic POD - reduced-dynamic POD - onboard POD - POD with Integer Ambiguity Resolution

Introduction

The Low Earth Orbit (LEO) satellites, including CubeSats, have an orbital altitude that ranges from 300 to 1500 km. They are used in different space missions, including satellite gravimetry, Interferometric Synthetic Aperture Radar (In-SAR), GNSS radio occultation, satellite altimetry, global Earth mapping and monitoring, formation flying, and positioning using mega-constellations. Orbits with high accuracy, mainly at the sub-dm level, are required for almost all these missions (Montenbruck 2017). Precise Orbit Determination (POD) methods are categorized into three main types: dynamic, kinematic, and reduced-dynamic POD.

The dynamic POD incorporates dynamic models of forces that affect the satellite motion. Such models are used to solve the satellite equation of motion (Eq. 1) using numerical integration to determine the best-fitting orbit. The equation of motion for a LEO satellite can be considered as a second-order differential equation relating its movement to the accelerations ($\mathbf{a}$) that perturb the orbit. These perturbation accelerations depend on time (t), position ($\mathbf{r}$), velocity ($\mathbf{v}$), and physical forces ($\mathbf{f}$) affecting the motion. The equation of motion is expressed as (Dach et al. 2015):

$$\frac{d^2\mathbf{r}}{dt^2} = \mathbf{a}(t, \mathbf{r}, \mathbf{v}, \mathbf{f}) = -GM\frac{\mathbf{r}}{\|\mathbf{r}\|^3} + \mathbf{a_p} \quad (1)$$

where $\mathbf{a}$ is the total acceleration, GM is the product of the gravitational constant and the mass of the Earth, the vector $\mathbf{r}$ denotes the position vector of LEO satellite and $\|\cdot\|$ forms the norm of a vector. The first term on the right side of Eq. 1 is the central gravity term, which has the dominant effect on the LEO satellite. The other perturbations represented as $\mathbf{a_p}$, are caused by other physical forces that

[1] School of Earth and Planetary Sciences, Curtin University, Perth, Australia (corresponding author).
Email: amir.allahvirdizadeh@curtin.edu.au;
[2] School of Earth and Planetary Sciences, Curtin University, Perth, Australia; National Time Service Center, Chinese Academy of Sciences, Xi'an, China; University of Chinese Academy of Sciences, Beijing, China
Email: wangkan@ntsc.ac.cn
[3] School of Earth and Planetary Sciences, Curtin University, Perth, Australia.
Email: A.El-Mowafy@curtin.edu.au

impact the LEO motion. These forces are categorized into gravitational ($\mathbf{f_g}$) and non-gravitational ($\mathbf{f_{ng}}$) forces. The gravitational forces include higher-order terms of the Earth gravity ($\mathbf{f_{ho}}$), the gravitational attractions by the Sun, Moon, and the other celestial planets ($\mathbf{f_{smp}}$), the solid earth, pole and ocean tidal effects ($\mathbf{f_{ti}}$), and the general relativistic effects ($\mathbf{f_{rel}}$), combined into the following equation:

$$\mathbf{f_g} = \mathbf{f_{ho}} + \mathbf{f_{smp}} + \mathbf{f_{ti}} + \mathbf{f_{rel}} \quad (2)$$

The non-gravitational forces are independent of the satellite mass and include the atmospheric drag ($\mathbf{f_d}$), solar radiation pressure (SRP) denoted as ($\mathbf{f_r}$), and the Albedo effect ($\mathbf{f_{al}}$) as follows:

$$\mathbf{f_{ng}} = \mathbf{f_d} + \mathbf{f_r} + \mathbf{f_{al}} \quad (3)$$

The atmospheric drag is the friction of the satellite with the Earth atmosphere, the SRP is the acceleration due to the absorption or reflection of solar photons, and the Albedo effect is caused by the solar energy flux reflected from the Earth. The above forces are discussed in detail in Montenbruck and Gill (2000) and approximate values of these accelerations on an example of LEO satellites are given in Table 32.2 in Montenbruck (2017). To solve the equation of motion and achieve precise orbits, arc-by-arc, different stepwise numerical integration methods are used (Montenbruck and Gill 2000).

The accuracy of the dynamic POD is highly dependent on the accuracy of physical force models used, and the deficiencies in these models cause systematic errors in the POD that grow with the arc length. These deficiencies are related mostly to the non-gravitational part, including atmospheric drag and SRP. Accurate modeling of the atmospheric drag depends on the accuracy of the information on the density of the upper atmosphere, the detailed knowledge of the interaction of the atmospheric particles with the satellite surface, and the satellite attitude in space. The SRP depends on the satellite shape, the surface coating materials, and the orientation. These dependencies cause accuracy degradation in the dynamic POD for the LEO satellites, because the drag and SRP coefficients should be estimated during the POD to model these accelerations accurately, which is not happening for the purely dynamic POD. Therefore, the kinematic POD using only GNSS measurements, and the reduced-dynamic POD that uses both dynamic models and GNSS observations, have been developed during the previous two decades to improve the orbital accuracy of LEO satellites.

In this paper, the kinematic and the reduced-dynamic POD using undifferenced measurements are discussed and compared in detail in the next section from the post-mission viewpoint and based on the batch least-squares solution. For each method, the functional, stochastic, and dynamic models, as well as the pre-processing, post-mission solution, and validation steps are given. The concept of real-time POD based on filtering is discussed in the following section “Real-Time POD”. At the end of each section, a discussion about the latest studies related to each topic is provided. Finally, an outlook on the POD of LEO satellites based on undifferenced GNSS observations along with a comparison of the discussed methods is given in the conclusion. A flow diagram of the paper structure including the section headings is provided in Figure 1 to help the readers follow the content.

Post-mission POD

The post-mission precise LEO orbits are essential in many geoscience applications. Depending on the applications, the precise orbits may be available with different latencies, from several hours for weather forecasting or urgent satellite imagery, to several days for non-emergency applications that require the highest possible accuracy. The POD of such missions is performed in processing centers using different software packages such as GipsyX from the Jet Propulsion Laboratory (JPL) (Bertiger et al. 2020), Bernese GNSS Software from the Astronomical Institute of the University of Bern (AIUB) (Dach et al. 2015), GHOST from the German Space Operations Center (DLR) (Wermuth et al. 2010), and PANDA from the Wuhan University (Chuang et al. 2008). In this section, a general algorithm for the post-mission POD based on the kinematic and reduced-dynamic methods is discussed. The main issues and questions that the reader could encounter in post-mission POD are summarized in Figure 2 and are discussed below.

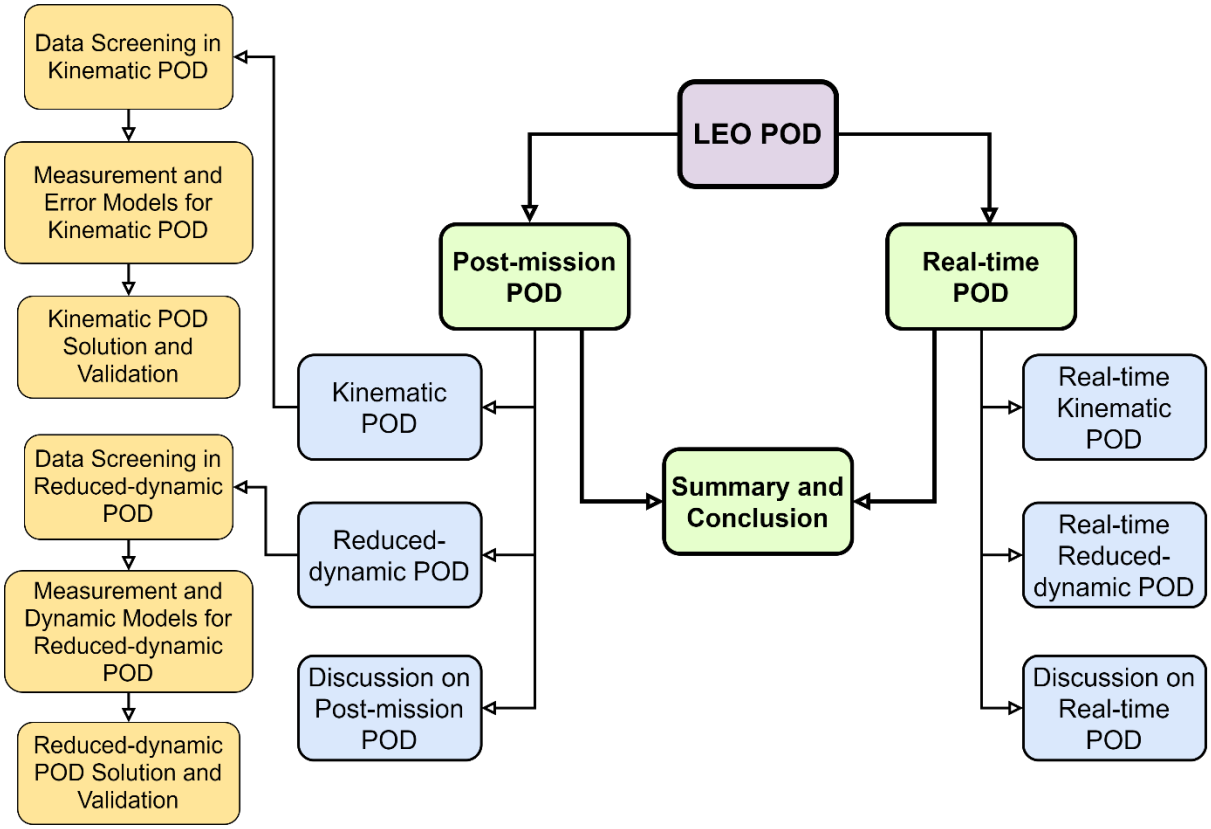

Fig. 1. Flowchart of the paper structure.

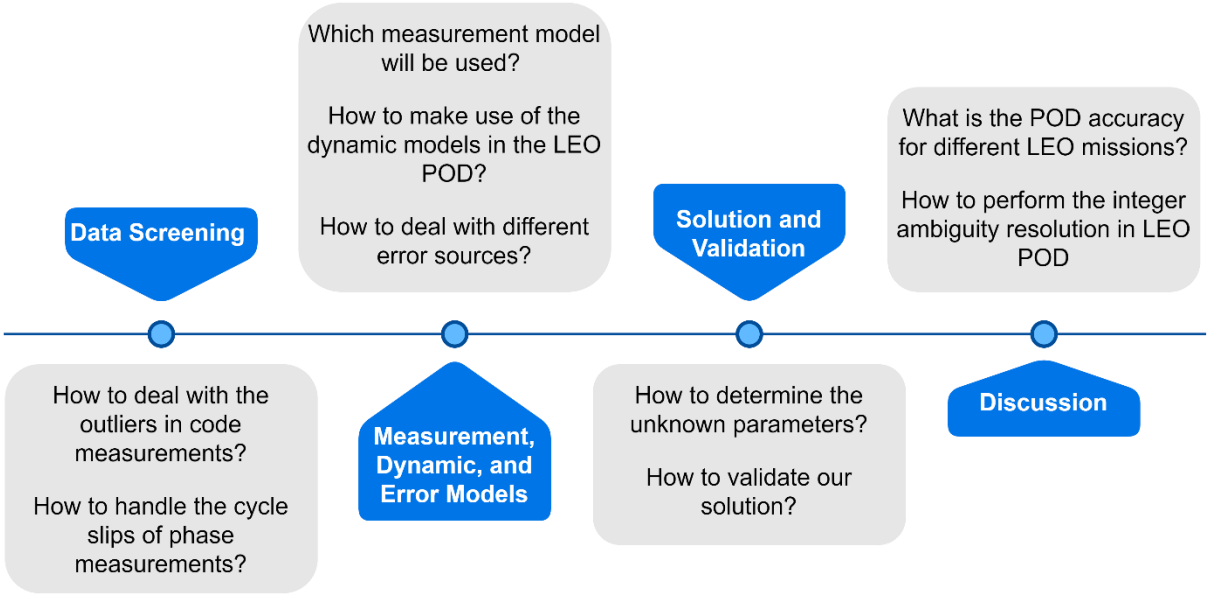

Fig. 2. Questions that will be addressed in each section.

Kinematic POD

The kinematic POD method estimates the orbit by processing only the GNSS measurements with a precise positioning approach without considering the dynamic models. Hence, it is susceptible to satellite geometry, measurement errors, noise, and data outages and orbit estimation will not be accurate or even available when the GNSS data have large biases or gaps. This something could happen in small LEO satellites with limited power capability, such as CubeSats (Wang et al. 2020).

Kinematic POD is a popular method in recovering the gravity field information, as the a-priori knowledge of the involved physical forces is not required (Jäggi et al. 2016). The use of this method for the gravity field determination was demonstrated by Švehla and Rothacher (2003a), and the first gravity field model based on kinematic orbits was calculated in Gerlach et al. (2003).

The kinematic POD in post-mission mode starts with the quality control of the observations, followed by orbit determination based on the precise point positioning (PPP) approach. These steps are discussed below.

Data Screening in Kinematic POD

The orbital periods of LEO satellites are around 90-120 minutes, where a typical GPS satellite is visible for them for less than 40 minutes (Ren and Schön 2018). This short period is due to the low orbital altitude of the LEO satellite and its higher velocity ($\sim 8\ \mathrm{km/s}$) than the GNSS satellites ($\sim 4\ \mathrm{km/s}$). During this period, weak GNSS signals and the possible ionospheric scintillations may cause signal loss-of-lock and cycle slips, which would reduce the strength of the model. As such, to achieve precise kinematic orbits, the GNSS measurements should be pre-processed through, e.g., the so-called Fault Detection and Exclusion (FDE) method (El-Mowafy 2014).

The FDE concept is based on testing the null hypothesis that expresses the error-free model against the alternative hypotheses that refer to the possibility of the presence of outliers in observations. It can be summarized as follows:

- Detecting the presence of outliers in observations using the overall test statistic $T_q = \hat{\mathbf{e}}^{\mathrm{T}}\mathbf{Q}_{\mathbf{y}}^{-1}\hat{\mathbf{e}}$ which follows a central Chi-square distribution in the fault-free mode. $\hat{\mathbf{e}}$ denotes the observation residuals, assumed to be normally distributed, and $\mathbf{Q}_{\mathbf{y}}$ denotes the covariance matrix of the observations. If $T_q \geq \chi^2_\alpha(df, 0)$, the null hypothesis is rejected, indicating the presence of outliers. $\chi^2_\alpha(df, 0)$ represents the central Chi-square distribution function for a pre-defined significance level α and the observations degrees of freedom df.
- Identifying the observation that causes this model error using, e.g., Baarda w-test statistic (Baarda 1968). The identified code observation will be excluded from the rest of the processing, and a new ambiguity will be introduced in the unknown vector for the identified phase observation.

Besides the FDE method, there are other approaches for the cycle slip detection that can be considered for the POD of LEO satellites (See e.g. Ren and Schön (2018)).

Measurement and Error Models for Kinematic POD

A simplified measurement model for code (P) and phase observations (Φ) between the GNSS satellite s and the LEO spaceborne receiver r at frequency j is expressed as:

$$\begin{aligned} P^s_{r,j} &= \rho^s_r + c(dt_r - dt^s) + \mu_j I^s_{r,1} + c\left(d_{r,j} - d^s_j\right) + e_j \\ \Phi^s_{r,j} &= \rho^s_r + c(dt_r - dt^s) - \mu_j I^s_{r,1} + c\left(\delta_{r,j} - \delta^s_j\right) + \lambda_j n^s_{r,j} + \epsilon_j \end{aligned} \tag{4}$$

where ρ^s_r denotes the receiver-satellite range in meters. The speed of light is indicated by c in m/s, and dt_r and dt^s express the receiver and satellite clock offsets in seconds. $\mu_j = f_1^2/f_j^2$ is the unitless coefficient to be multiplied with the ionospheric delay on L1 ($I^s_{r,1}$ in meters) for the frequency f_j. The receiver code and phase hardware biases are denoted by $d_{r,j}$ and $\delta_{r,j}$, and the satellite code and phase hardware biases are indicated by d^s_j and δ^s_j, respectively, which are expressed in seconds. The receiver code hardware biases are lumped with the receiver clocks, and the phase hardware biases, which are considered constant in time, are lumped with ambiguities. The phase ambiguity parameter $n^s_{r,j}$ is transformed from cycles to the range by multiplying with the wavelength λ_j. Noises and remaining miss-modeled errors such as multipath are denoted by e_j and ϵ_j for code and phase, respectively. The shape of the solar panels and the position of the patch antenna are two main sources of multipath error for the LEO satellites. The tropospheric delays are not present for the LEO satellites

due to their altitudes (Hofmann-Wellenhof et al. 2008). For the multi-GNSS receivers, the inter-system biases (ISBs) need to be considered in the processing to compensate for differences in time references and hardware biases between GNSSs (Kouba et al. 2017).

GNSS precise orbits and clocks

Precise GNSS orbits and clocks are essential for POD since using the broadcast ephemeris can deliver POD accuracy at the meter to sub-meter (Montenbruck and Ramos-Bosch 2008). This precise information is available from, e.g., International GNSS Service (IGS) or Center for Orbit Determination in Europe (CODE) with different sampling intervals. Note that the higher-order Lagrange polynomials can be used to interpolate the GNSS satellite orbits with the large sampling intervals of e.g., 15 min (Feng and Zheng 2005), but interpolating clocks could degrade their accuracy dramatically. As such, analysis centers like the CODE also deliver high-rate clock products. The high-sampled clocks also deliver the possibility to access the short-term stability of the onboard clocks, which is crucial for different applications (Hauschild et al. 2013).

Antenna Phase Center

The LEO satellite antenna phase center offsets (PCOs) and phase center variations (PCVs) can be determined from the consistent nominal antenna models achieved before the launch using a robotic measurement system (Montenbruck et al. 2009). However, these models do not reflect the actual space environment, such as experiencing the effect of the near-field multipath. Neglecting or incorrect modeling of the antenna PCOs and PCVs could cause systematic errors in the LEO POD. To compensate for this limitation and generate the correct phase center pattern to improve the consistency of the POD solutions, the LEO observations can be used in the empirical inflight calibration methods, i.e., the so-called “residual” and “direct” approaches. In the residual approach, phase residuals are used to derive the empirical PCVs as bin-wise mean values, while in the direct approach, the PCV values are considered as the unknowns and estimated in the processing (Jäggi et al. 2009). As an example, Van Den Ijssel et al. (2015) used the residual approach to derive PCVs for the Swarm constellation.

Ionospheric errors

There are two main approaches to deal with the ionospheric error in the POD process. The first approach removes the first-order term of the ionospheric delay by forming the ionosphere-free (IF) linear combination using dual-frequency GNSS measurements. This combination increases the noise level by a factor of $\sqrt{(f_i^4 + f_j^4)/(f_i^2 - f_j^2)^2}$, e.g., approximately three orders of magnitude for L1 and L2. The corresponding GNSS satellite differential code biases (DCBs) need to be considered if the formed IF combination is different from the one contained in the precise GNSS satellite clocks. Despite using the IF combination, the higher-order ionospheric terms are not removed. The magnitude of these terms is in the range of few millimeters to several centimeters, depending on the solar activity conditions, the carrier frequency, and the relative orientation of the LEO satellite to the magnetic field (Hoque and Jakowski 2007). These errors are generally neglected in most POD processing approaches. The second approach in dealing with the ionospheric delay is to use the uncombined measurements and estimate ionospheric delays as the unknown parameters. It allows for extensions to an arbitrary number of frequencies and could strengthen the model by implementing the spatial and temporal constraints on the ionospheric parameters (Odijk et al. 2016). Since the first approach, i.e., forming IF combination, is used in most POD studies, it will be used in the rest of this paper.

Regardless of the method used to deal with the ionospheric delay, the ionospheric scintillation can degrade or even interrupt the GNSS tracking (Kintner et al. 2007). Such performance reduction is observed in the Swarm GPS receiver, and several modifications, in the tracking loop and the antenna field of view were performed after launch to solve the problem (Van den Ijssel et al. 2016).

Unknown parameter Vector

The unknown parameter vector in the post-mission kinematic POD is defined as $\mathbf{x} = (\mathbf{r}^T, dt, \mathbf{b}^T)^T$ where for epoch t with m satellites, the vector $\mathbf{r} = (x_t, y_t, z_t)^T$ is the LEO satellite position, the term dt contains the LEO clock offsets in range and $\mathbf{b} = \left(b_t^{S_1}, \dots, b_t^{S_m}\right)^T$ includes the IF ambiguities that are lumped with the corresponding hardware biases.

Kinematic POD Solution and Validation

Estimation

To determine the unknown parameters at epoch t (for $t = 1, \dots, k$), the IF combination of code (P_{IF}) and phase (Φ_{IF}) measurements are considered in the observation vector $\mathbf{y} = (\mathbf{y}_1^T, \mathbf{y}_2^T, \dots, \mathbf{y}_k^T)^T$, where $\mathbf{y}_t = (P_{IF}^T, \Phi_{\mathrm{IF}}^T)^T$. In a batch least-squares estimation, the observation linearized model is expressed as:

$$\mathrm{E}\{\Delta\mathbf{y}\} = \mathbf{J}\Delta\mathbf{x}; \qquad \mathrm{D}\{\Delta\mathbf{y}\} = \mathbf{Q}_{\mathbf{y}} \tag{5}$$

where E and D denote the mathematical expectation and dispersion operators, respectively. $\mathbf{J}$ is the partial derivative of the observations concerning the unknown parameters that form the design matrix. Different observation weighting models including the equal and the elevation-dependent weighting models are often applied to form the variance-covariance matrix of the observations $\mathbf{Q}_{\mathbf{y}}$. However, giving equal weights to all observations may not be optimal for all satellites and the correct calculation of the elevation angels requires the attitude information recorded by the satellites that may not be available for low-power satellites. Using a weighting model based on signal-to-noise ratio is a possible solution that is proposed by Allahvirdi-Zadeh et. al (2021). Equation 5 can be efficiently solved using the parameter pre-elimination and back-substitution.

Validation

After the data screening and the processing steps, the output orbits should be validated using internal and external validation methods. The internal validation method uses a precise reference orbit, which can, e.g., be prepared from the reduced-dynamic POD method with the single-difference integer ambiguity resolution. Besides, the overlap analysis between subsequent orbits is often used to assess the internal consistency (Montenbruck 2017). In this method, two orbits (arcs) are generated while they have time overlap, e.g., daily arcs that are 30 hours long. The differences between two orbits in the overlapping period should be small enough to validate the processing results.
The external validation method uses the non-GNSS technique such as the Satellite Laser Ranging (SLR) and K-band ranging (KBR) system to compare the measured range with that computed from the POD (Arnold et al. 2019). Some LEO altimetry missions such Sentinel-3, which require high accuracy in the radial direction, are equipped with a Doppler Orbitography and Radiopositioning Integrated by Satellite (DORIS) antenna (Auriol and Tourain 2010). It can be used for both the DORIS POD and as an external validation tool (Fernández 2019).

The external validation methods are mainly available for the large LEO satellites such as GOCE (Bock et al. 2014) and Sentinel-3 (Fernández et al. 2016) that are equipped with the required costly sensors. This may not be possible for small satellites, such as CubeSats. The internal validation and self-consistency POD tests, such as the analysis of residuals and the orbit overlaps, are thus considered for these satellites.

Reduced-dynamic POD

As discussed before, the dynamic and kinematic POD have some limitations. The former requires comprehensive dynamic models that are not precisely available for the LEO satellites (especially the non-gravitational force models), and the latter is sensitive to data outages and weak GNSS satellite geometry. The reduced-dynamic POD, however, can benefit from both sides, i.e., the availability of dynamic models, as well as GNSS observations. In this method, the initial conditions, the force model parameters and possible stochastic accelerations are estimated instead of the epoch-wise LEO positions in the kinematic POD.

Since this POD method delivers more accurate orbital positions than the other two approaches, it has been used as the primary method to determine the orbit of different LEO missions, such as TOPEX/Poseidon (Yunck et al. 1994), CHAMP (Švehla and Rothacher 2003a) Jason-1 (Haines et al. 2004), GRACE (Kang et al. 2003), GOCE (Bock et al. 2014), Swarm (Van Den Ijssel et al. 2015), HY-2A (Guo et al. 2015), FY-3C (Zhang et al. 2018), Sentinel (Fernández 2019), and GRACE-FO (Kang et al. 2020). In the following, different steps of this approach are discussed.

Data Screening in Reduced-dynamic POD

As explained in the section "Data Screening for Kinematic POD", similar methods can be performed to screen GNSS data before starting the POD processing. However, some POD software packages, such as Bernese, perform the data screening step along with the POD steps. Such procedure is mentioned in the Section "Reduced-dynamic POD Solution and Validation", Step 2.

Measurement and Dynamic Models for Reduced-dynamic POD

Based on the measurement models given in Eq. 4, the LEO receiver clocks and ambiguities are estimated together with the elements used to propagate the LEO orbits, i.e., the satellite initial conditions, the force model parameters and possible stochastic accelerations. The latter two terms can be used to form the improved orbital accelerations. The dynamic model, expressed by the equation of motion (Eq. 1), is a second-order differential equation. With the unknowns mentioned above estimated in a least-squares adjustment, the LEO satellite trajectory can be propagated for any arbitrary time point with the improved accelerations and the initial state vector $\mathbf{S_0} = (\mathbf{r_0}^T, \mathbf{v_0}^T)^T$, by using numerical integration of the equation of motion. The initial position $\mathbf{r_0}$ and velocity $\mathbf{v_0}$ vectors, can be defined based on Keplerian elements (Dach et al. 2015).

Variational Equations

Due to the non-linearities, the partial derivatives of the state vector at an arbitrary time t with respect to the initial state vector and the force model parameters need to be numerically integrated. These partials represent a transition matrix $\tilde{\mathbf{\Phi}} = \partial_{\mathbf{S_0}}\mathbf{S_t}$, which is the partial derivatives of the current state using the initial state vector, and a sensitivity matrix $\tilde{\mathbf{S}} = \partial_{\mathbf{p}}\mathbf{S_t}$, which is the partial derivatives with respect to the force model parameters $\mathbf{p}$. They can be computed using numerical integration of the following so-called variational equations (Montenbruck and Gill 2000):

$$\begin{aligned}\frac{d}{dt}(\tilde{\mathbf{\Phi}}, \tilde{\mathbf{S}}) &= \begin{pmatrix} \partial_{\mathbf{r}}\mathbf{v} & \partial_{\mathbf{v}}\mathbf{v} \\ \partial_{\mathbf{r}}\mathbf{a} & \partial_{\mathbf{v}}\mathbf{a} \end{pmatrix}_{6\times 6} (\tilde{\mathbf{\Phi}}, \tilde{\mathbf{S}}) + \begin{pmatrix} \mathbf{0} & \partial_{\mathbf{p}}\mathbf{v} \\ \mathbf{0} & \partial_{\mathbf{p}}\mathbf{a} \end{pmatrix}_{6\times(6+n_{\mathbf{p}})} \\ &= \begin{pmatrix} \mathbf{0} & \mathbf{I} \\ \partial_{\mathbf{r}}\mathbf{a} & \partial_{\mathbf{v}}\mathbf{a} \end{pmatrix}_{6\times 6} (\tilde{\mathbf{\Phi}}, \tilde{\mathbf{S}}) + \begin{pmatrix} \mathbf{0} & \mathbf{0} \\ \mathbf{0} & \partial_{\mathbf{p}}\mathbf{a} \end{pmatrix}_{6\times(6+n_{\mathbf{p}})}\end{aligned} \tag{6}$$

where $n_{\mathbf{p}}$ is the number of the dynamic parameters estimated during the orbit determination, to account for effects like the atmospheric drag and SRP. Note that $\partial_{\mathbf{r}}\boldsymbol{v}$ is zero since $\mathbf{r}$ and $\mathbf{v}$ are two independent components in the state vector. Likewise, $\mathbf{v}$ does not depend explicitly on $\mathbf{p}$, and $\partial_{\mathbf{p}}\mathbf{v}$ is zero. This variation equation is numerically integrated by using existing force models and improved model parameters (in the last iteration) to generate the corresponding partial derivatives at an arbitrary time point. Examples of the existing force models are given in Table 1.

Empirical Accelerations

Despite using available force models, deficiencies could still exist in the models for the SRP and air drag. For example, the drag force model depends on the satellite body (shape, size, and orientation), the distribution of atmospheric layer density, and the predictive assessment of this density (Vallado and Finkleman 2014). The possible model deficiencies can thus be compensated by using empirical accelerations (Montenbruck et al. 2005). The empirical accelerations are estimated in

the orbit determination procedure as the unknown parameters in the radial $\boldsymbol{\alpha_R}$, along-track $\boldsymbol{\alpha_{AT}}$, and cross-track $\boldsymbol{\alpha_{CT}}$ directions. They can be lumped in the term $\boldsymbol{\alpha_{EMP}}$ as follows:

$$\boldsymbol{\alpha_{EMP}} = \boldsymbol{\alpha_R}\,\mathbf{e_R} + \boldsymbol{\alpha_{AT}}\,\mathbf{e_{At}} + \boldsymbol{\alpha_{CT}}\,\mathbf{e_{CT}} \tag{7}$$

where $\mathbf{e_R}$, $\mathbf{e_{CT}}$, $\mathbf{e_{AT}}$ represent the unit vectors in the radial, cross-track, and along-track directions, respectively. The accelerations can be estimated as piecewise constants for a time interval ($t_{i-1} \leq t < t_i$) (Jäggi et al. 2005). The drawback of this concept is that the changes in the improved orbit are not differentiable at t_i. Therefore, the concept of piecewise-linear accelerations was introduced by Jäggi et al. (2006) to overcome this limitation and allow to set up continuous piecewise accelerations, which improves orbital accuracy. As an alternative approach, small velocity changes at the pre-defined epochs, the so-called pseudo-stochastic pulses, can be estimated. However, the improvement could be discontinuous at the time epochs introducing the pulses (Jäggi et al. 2006).

Stochastic parameters in the reduced-dynamic POD can be parametrized as a combination of the above-mentioned approaches. One procedure, which is used in the GHOST POD package, starts with computing SRP and drag accelerations using simple models (See Table 1), then adjusts scale factors (coefficients) for these accelerations during the orbit determination, and finally estimates the piecewise-constant empirical accelerations for the pre-defined sub-intervals to compensate for model deficiencies. Another possible procedure, e.g. that used in the Bernese GNSS software, is based on different parameterizations of the stochastic parameters in the different processing steps of the reduced-dynamic POD procedures. This procedure is explained in the following section.

Reduced-dynamic POD Solution and Validation

The post-mission solution of the unknown parameters can be performed with the following steps, taking the example of the Bernese GNSS software for the LEO POD using dual-frequency GPS observations, with a flowchart of these steps shown in Figure 3:

Step 1: The solution starts from a single point positioning using code observations passing the outlier detection step. The collocation method, as the numerical integration method in Bernese (Dach et al. 2015), is then used to generate a code-based reduced-dynamic orbit, fitting the kinematic positions. These outputs will be used for the GNSS phase observations pre-processing in the following step.

Step 2: Phase observations are screened and used to improve the orbital accuracy in an iterative process. The entire orbit is divided into $n_{\boldsymbol{\alpha}}$ intervals with equal time periods, and in each iteration, the stochastic velocity changes are determined for each interval. For a LEO satellite with an orbital period of 90-120 min and the GNSS measurements with a sampling interval of 10-30 s, the orbit interval could be set to, e.g., 15 min. The estimated velocity pulses are used along with the estimated initial conditions and force model parameters in a numerical integration step to improve the orbit. The updated orbit in the last iteration and the screened phase data will be used in the final reduced-dynamic POD.

Step 3: In the final POD, another round of least-squares estimation is performed using the fault-free phase observations and considering reduced time intervals, e.g., from 15 min to 6 min, to estimate piecewise constant accelerations. The numerically integrated orbit is considered as the final reduced-dynamic orbit.

The validation methods discussed in the section “Kinematic POD Solution and Validation” can also be used to validate the final reduced-dynamic orbit.

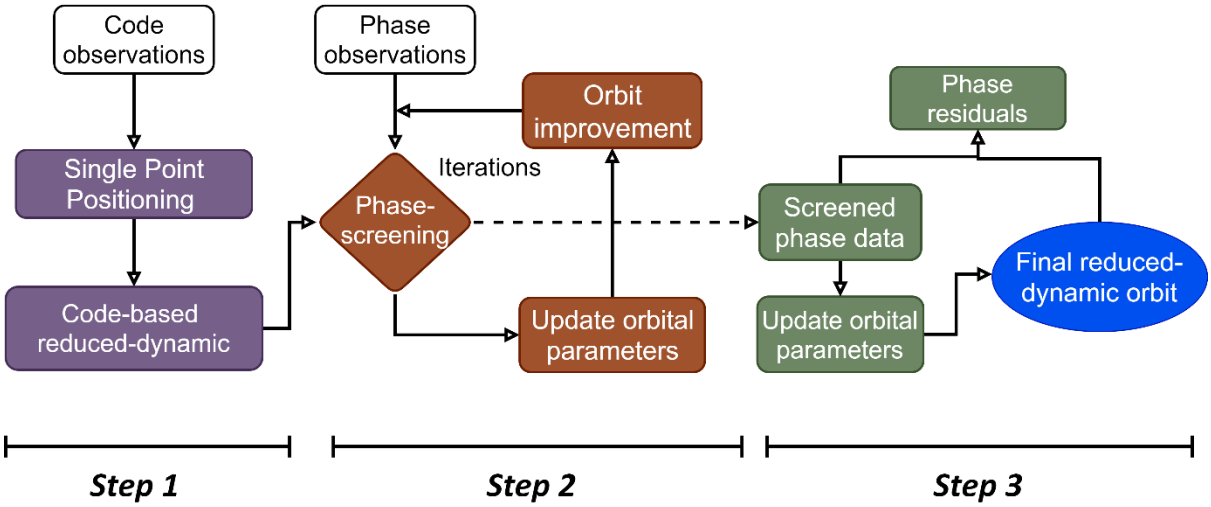

Fig. 3. Flowchart of reduced-dynamic POD computation procedure.

Discussion on Post-mission POD

The kinematic and the reduced-dynamic POD using single- and dual-frequency observations are used in different LEO satellite-related studies. Table 2 presents a selection of LEO POD accuracies achieved with the different validation methods, based on undifferenced dual-frequency measurements with both the kinematic and reduced-dynamic methods used in different missions. These results were obtained from different studies over a rather long timespan (2005-2020). The presented POD accuracies are therefore affected by the progress in the gravitational force modeling, achieved by different gravity field missions over these years. Note that satellites in higher orbits often have lower RMS errors, mainly due to the harsh dynamical environment of satellites in the lower altitudes (e.g., Swarm-B satellite in Table 2 that has a higher altitude than Swarm-A and -C).

The orbital accuracy of the kinematic POD method is correlated to the epoch-wise receiver clock offset determination. There is a high correlation between the radial component of the orbit and the receiver clock parameters (Weinbach and Schön 2012). Stable oscillators thus enable a robust clock model and can stabilize the radial orbital component. This concept is simulated for the GRACE mission to model the receiver clock offset, and a 40% improvement in the radial direction is shown (Yang et al. 2014).

In all the studies discussed above, the first-order ionospheric delay is removed by forming the IF linear combination. However, as discussed in the section “Measurement and Error Models of Kinematic POD”, the uncombined observations can also be applied in the POD. The kinematic POD with raw measurements, considering the higher-orders of the ionospheric delays provided similar orbital accuracy compared with using the IF combination (Zehentner and Mayer-Gürr 2016).

Although this paper reviews LEO POD methods based on using undifferenced GNSS measurements, it is worth mentioning that differencing of the GNSS observables were also used for LEO POD, where GNSS observations collected on a LEO satellite are differenced with GNSS observations at a known ground reference station. The double differencing of GPS phase measurements with ambiguity resolution for the kinematic POD of CHAMP was carried out by Švehla and Rothacher (2003b). The double differences (DD) were formed between the IGS permanent stations and the LEO satellite to reduce the orbit- and clock-related errors from the observation model. However, with such long baselines, the remaining orbital and clock errors still need to be considered. Besides, tropospheric errors need to be considered for the observations at the ground stations. Furthermore, the concept of DD between two GRACE satellites formed the first GPS baseline in space with the mm-accuracy after performing ambiguity resolution (Švehla and Rothacher 2004). Such baseline can be used for the orbit validation and gravity recovery in GRACE-FO mission (Kang et al. 2020).

Integer Ambiguity Resolution in Post-mission LEO POD

Single receiver Integer Ambiguity Resolution (IAR) can effectively improve the positioning accuracy; however, it requires corrections for the hardware biases to recover the integer nature of the ambiguities. Different IAR methods were reviewed comprehensively in Teunissen and Khodabandeh (2015). Among the available single-receiver-based IAR methods, the methods proposed by Laurichesse et al. (2009) and Bertiger et al. (2010) are usually used for the LEO POD. The former method is based on identifying the satellite wide-lane biases, using them to estimate the undifferenced wide-lane ambiguities for a network, and finally fixing L1 ambiguities for these receivers. A similar approach has been tested for GRACE and Jason-1, i.e., their wide-lane measurements were corrected by the GPS fractional wide-lane corrections provided by the network. Next, the GPS satellite integer clocks derived from the network were used to estimate the IF phase residuals. Finally, by forming between-satellite single differences of these residuals, the receiver clock offset was removed and the integer ambiguities were estimated. The orbits of these satellites determined by the unambiguous measurements were shown to be more accurate than the orbits from float solutions, i.e. those estimated with float ambiguities. In the method proposed by Bertiger et al. (2010), GPS orbit errors and clock offsets, dual-frequency phase biases, and corresponding wide-lane values were estimated in a network solution and were used to form integer constraints in the LEO data processing. The method has been tested for the Jason-2 mission, and it was shown that the radial orbital accuracy increased significantly, i.e., reaching below 1 cm, fulfilled the altimetry requirements. The wide-lane ambiguities have a longer wavelength than the original ambiguities, which eases the ambiguity resolution by reducing the number of potential ambiguity candidates. In addition to the methods mentioned above, the IAR for Sentinel-3A data has been performed by Montenbruck et al. (2018) using the wide-lane bias products and the integer phase clock offset corrections from the Centre National d'Etudes Spatials (CNES). The orbit generated with fixed ambiguities outperformed the orbit of float solutions. The RMS value (validated by the SLR) reached 5 mm, which has a 30% improvement. The systematic biases in the cross-track direction were also revealed through the IAR due to the errors in the antenna PCOs, which can be absorbed by the ambiguities in the float solution.

In addition to the kinematic and the reduced-dynamic methods, a fourth POD approach was introduced by Švehla and Rothacher (2005a) called the reduced-kinematic POD. However, it has not been developed further since it was used inside the kinematic POD only for the gravity field determination (Švehla 2018).

In summary, both the kinematic and the reduced-dynamic POD in the post-mission processing can deliver orbital accuracy at cm-level, which can be improved by the IAR. This accuracy fulfills the requirements of most post-processed LEO applications (Montenbruck 2017). The reduced-dynamic POD makes use of the strong dynamic models and can normally deliver higher orbital accuracy than the kinematic mode. However, the extensive dynamic modeling requires high computational load, which is not a big issue in post mission by the ground-based processing centers, but could be an issue for onboard processing, especially for small satellites, such as CubeSats.

Real-time POD

The real-time POD of LEO satellites is an essential requirement for their control and guidance. It provides a valid link between the data collected using the onboard sensors and the ground monitoring stations that support data collection and facilitate dissemination. However, there are some challenges in the onboard POD. For example, due to the limited power and memory budget, especially for small LEO satellites such as CubeSats, the onboard algorithms should consider the trade-off between the computational load, onboard power resources, and the required orbit accuracy (Montenbruck and Ramos-Bosch 2008). Therefore, using dynamic models with a high degree and time/memory-consuming estimation approaches, such as the batch least-squares adjustment, might not be preferable for CubeSats. One thus often needs to simplify the dynamic model by, e.g., utilizing the Earth's gravity model with a lower degree, and perform the POD based on a real-time filter. The same

applies to additional information, e.g. the attitude information, which requires more sensors and payload, but would be important for achieving good accuracy and availability of the POD results.
The real-time POD algorithms are based on recursive methods for the nonlinear models, including the Extended Kalman Filter (EKF) and the Unscented Kalman filter (UKF). The EKF method is based on linearization of the dynamic and measurement models, whereas the UKF approach relies on a nonlinear transformation (the so-called unscented transformation) to propagate the mean and covariance information without using linearizing models. The UKF is developed for highly nonlinear problems, but the real-time filter performs close to linearity if proper initial conditions and accurate force models are considered in the filter (Montenbruck 2017). Therefore, the EKF method, as the most common method used in the onboard POD, is explained in this paper. It is followed by a discussion about the limitations of the real-time POD and the latest studies in this field. The algorithms for the orbit determination based on UKF were explained in, e.g., Pardal et al. (2010).

Real-time Kinematic POD

The state vector for the kinematic POD at each epoch t is expressed as $\mathbf{x} = (\mathbf{r}^T, dt, \mathbf{b}^T)^T$. The processing is initialized with the initial values of the filter state ($\mathbf{x_0}$) and its covariance matrix ($\mathbf{Q_0}$), which are typically estimated using the least-squares adjustment. Since no dynamic model was used in the kinematic POD, an identity matrix is considered as the transition matrix ($\boldsymbol{\phi}_t^{KIN} = \mathbf{I}$, where KIN refers to kinematic) to update the clock offset and ambiguities combined in $\hat{\mathbf{x}}'$ as follows:

$$\begin{cases} \hat{\mathbf{x}}'_{t|t-1} = \boldsymbol{\phi}_t^{KIN} \hat{\mathbf{x}}'_{t-1|t-1} \\ \widehat{\mathbf{Q}}^{\mathbf{x}'}_{t|t-1} = \boldsymbol{\phi}_t^{KIN} \mathbf{Q}^{\mathbf{x}'}_{t-1|t-1} \boldsymbol{\phi}_t^{KIN^T} + \mathbf{Q}_t^{KIN} \end{cases} \tag{8}$$

where the process noise matrix is diagonal, i.e. $\mathbf{Q}_t^{KIN} = diag(\sigma_{dt}^2, \sigma_{\mathbf{b}}^2)$ which represents the process noise of the clock offset modeled as random-walk, and the term $\mathbf{b}$ due to the hardware biases included in it. Note that if cycle slips take place the temporal link of the ambiguities is interrupted.

Before applying the measurement update, data screening process discussed in the section "Data Screening for Kinematic POD" should be performed. During the measurement update, the predicted states can be considered as pseudo-observations that aid GNSS observations of the current epoch and the unknowns can be estimated using a sequential least-squares adjustment, with the measurement and stochastic models expressed as:

$$\mathrm{E}\begin{pmatrix} \hat{\mathbf{x}}'_{t|t-1} \\ \mathbf{y}_t \end{pmatrix} = \begin{pmatrix} \mathbf{0} & \mathbf{I} \\ \mathbf{J_r} & \mathbf{J_{x'}} \end{pmatrix} \begin{pmatrix} \mathbf{r}_t \\ \mathbf{x}'_t \end{pmatrix}; \qquad \mathrm{D}\begin{pmatrix} \hat{\mathbf{x}}'_{t|t-1} \\ \mathbf{y}_t \end{pmatrix} = \begin{pmatrix} \widehat{\mathbf{Q}}^{\mathbf{x}'}_{t|t-1} & \mathbf{0} \\ \mathbf{0} & \mathbf{Q}_{\mathbf{y}_t} \end{pmatrix} \tag{9}$$

where $\mathbf{J_r}$ and $\mathbf{J_{x'}}$ represent the partial derivatives of the observations with respect to the kinematic orbits and the combined clocks and ambiguities, respectively. Note that although expressed in different forms, the above sequential least-squares adjustment is equivalent to EKF (Humpherys et al. 2010), provided that the same temporal link is considered.

Real-time Reduced-dynamic POD

The vector $\mathbf{x} = (\mathbf{r_0}^T, \mathbf{v_0}^T, \mathbf{p}^T, \boldsymbol{\alpha}_{\mathbf{EMP}}^T, dt, \mathbf{b}^T)^T$ is the EKF state vector in the reduced-dynamic POD, where $\mathbf{p} = (c_r, c_d)^T$ contains the SRP and drag coefficients. For m number of satellites, there are $12 + m$ unknowns at each epoch (6 satellite state components, 2 coefficients for the SRP and air drag, 3 empirical accelerations, 1 clock offset, and m phase ambiguities). The propagation in time update involves a simple integration method to compute both the satellite trajectory and the partial derivatives concerning the state vector and the term $\mathbf{p}$. The empirical acceleration parameters $\boldsymbol{\alpha}_{\mathbf{EMP}}$ are updated using a Gauss–Markov process, expressed as:

$$\boldsymbol{\alpha}_{\mathbf{EMP}_{t|t-1}} = l\, \boldsymbol{\alpha}_{\mathbf{EMP}_{t-1|t-1}} \quad \text{where} \quad l = e^{-\frac{|\Delta_{t,t-1}|}{\tau}} \tag{10}$$

$\Delta_{t,t-1}$ is the time difference between the current and previous epochs, τ is the time constant, and l is the exponential damping factor. Other state parameters of the filter remain constant during this

step with a white process noise model. Considering $\partial_{(x,y,z,v_x,v_y,v_z)}\,\boldsymbol{\alpha}_{\mathbf{EMP}_{t|t-1}} = \mathbf{0}$, and $\partial_{\boldsymbol{\alpha}_{\mathbf{EMP}_{t-1|t-1}}}\,\boldsymbol{\alpha}_{\mathbf{EMP}_{t|t-1}} = l$, the full structure of the reduced-dynamic EKF transitions matrix $\boldsymbol{\phi}_t^{RD}$, with the superscript *RD* denotes reduced dynamic, is expressed as:

$$\boldsymbol{\phi}_t^{RD} = \partial_{\mathbf{x}_{t-1|t-1}}\mathbf{x}_{t|t-1} = \begin{bmatrix} \tilde{\boldsymbol{\Phi}}_{6\times6} & \tilde{\mathbf{S}}_{6\times2} & \tilde{\mathbf{S}}_{6\times3} & \mathbf{0}_{6\times1} & \mathbf{0}_{6\times m} \\ \mathbf{0}_{2\times6} & \mathbf{I}_{2\times2} & \mathbf{0}_{2\times3} & \mathbf{0}_{2\times1} & \mathbf{0}_{2\times m} \\ \mathbf{0}_{3\times6} & \mathbf{0}_{3\times2} & l\times\mathbf{I}_{3\times3} & \mathbf{0}_{3\times1} & \mathbf{0}_{3\times m} \\ \mathbf{0}_{1\times6} & \mathbf{0}_{1\times2} & \mathbf{0}_{1\times3} & 1 & \mathbf{0}_{1\times m} \\ \mathbf{0}_{m\times6} & \mathbf{0}_{m\times2} & \mathbf{0}_{m\times3} & \mathbf{0}_{m\times1} & \mathbf{I}_{m\times m} \end{bmatrix}_{(12+m)\times(12+m)} \tag{11}$$

where $\tilde{\boldsymbol{\Phi}}$ and $\tilde{\mathbf{S}}$ are obtained from the numerical integration of the variational equation. The covariance update is expressed as:

$$\mathbf{Q}_{t|t-1} = \boldsymbol{\phi}_t^{RD}\mathbf{Q}_{t-1|t-1}{\boldsymbol{\phi}_t^{RD}}^T + \mathbf{Q}_t^{RD} \tag{12}$$

where the process noise matrix $\mathbf{Q}_t^{RD}$ is determined based on assumptions and simulations that are designed to prevent filter divergence. An example of such a matrix can be found in Montenbruck and Ramos-Bosch (2008), where the empirical accelerations and the receiver clock offsets were modeled using Gauss-Markov and the random walk processes, respectively.

Next, the measurement update is performed to improve the filter state vector with the newly available observations, after data screening and cycle slip detection process, as follows:

$$\begin{cases} \mathbf{K}_t = \mathbf{Q}_{t|t-1}\,\mathbf{J}_t^T\left(\mathbf{Q}_{\mathbf{y}_t} + \mathbf{J}_t\,\mathbf{Q}_{t|t-1}\,\mathbf{J}_t^T\right)^{-1} \\ \hat{\mathbf{x}}_{t|t} = \hat{\mathbf{x}}_{t|t-1} + \mathbf{K}_t\left(\mathbf{y}_t - \mathbf{j}_t(\hat{\mathbf{x}}_{t|t-1})\right) \\ \mathbf{Q}_{t|t} = (\mathbf{I}_m - \mathbf{K}_t\,\mathbf{J}_t)\mathbf{Q}_{t|t-1} \end{cases} \tag{13}$$

The gain matrix $\mathbf{K}_t$ depends on the covariance matrix of the measurements $\mathbf{Q}_{\mathbf{y}_t}$ and the propagated covariance from the time update step $\mathbf{Q}_{t|t-1}$. The term $\mathbf{J}_t$ is the partial derivative for the filter state vector and $\mathbf{j}_t(\hat{\mathbf{x}}_{t|t-1})$ contains the computed values of the observations.

Finally, an integration method, such as the 4th order Runge-Kutta (Butcher 2016), can be used to propagate the trajectory of the LEO satellite over a fixed time step to the desired output sampling interval (Montenbruck and Ramos-Bosch 2008). A flowchart of these steps is given in Figure 4. It is possible to simplify the above-mentioned algorithm to meet the computational budget of the small satellites such as CubeSats by considering drag and SRP coefficients as modeled values rather than estimating them, and not estimating empirical accelerations, as explained in Yang et al. (2016). However, it reduces the orbital accuracy to a meter level.

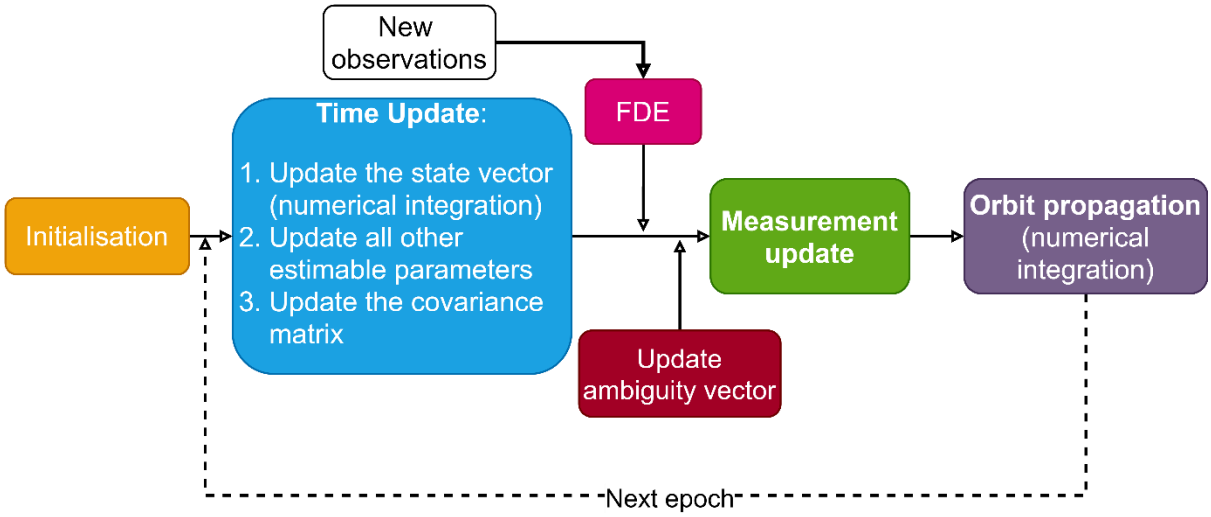

Fig. 4. Flowchart for the EKF reduced-dynamic POD

Discussion on Real-time POD

Different studies were carried out to overcome the limitations of real-time POD. One of these limitations is the poor accuracy of GPS orbits and clock offsets provided by the broadcast ephemeris. It was reported in Montenbruck and Ramos-Bosch (2008) that depending on the satellite altitude, an accuracy (defined by the daily 3D RMS) of 40-60 cm was achieved using GPS dual-frequency observations and broadcast ephemeris. The simulated multi-GNSS measurements from GPS, Galileo, and Beidou-3 satellites were tested in Hauschild and Montenbruck (2020) with a flight-proven algorithm developed by Montenbruck et al. (2008). It was reported that combining all measurements deliver LEO satellite orbits with 10.4 cm 3D RMS error when using broadcast ephemeris.

Real-time GNSS Precise Orbits and Clocks

One of the recent advancements of PPP is the availability of real-time GNSS precise orbit and clock corrections that can be provided by geostationary (GEO) satellites. There are some commercial services, such as G4 from Fugro (Tegedor et al. 2017) and TerraStar-D (Jokinen et al. 2014) that can provide such a service. In addition to the commercial services, the Japanese Quasi-Zenith Satellite System (QZSS) also provides the orbits and clock corrections through the L6 signal broadcast by the navigation satellites (IS-QZSS-L6-003 2020) within the Multi-GNSS Advanced Demonstration tool for Orbit and Clock Analysis (MADOCA) service. Moreover, the new-generation Australia/New-Zealand Satellite-Based Augmentation System (AU/NZ-SBAS) broadcasts real-time precise orbit and clock corrections to enable PPP through a GEO link (Barrios et al. 2018). These two free-of-charge services are available only over the Asia-pacific region. However, it is expected that such services can be available globally in the future by combining different SBASs and some by the new generation of GNSS (e.g. Galileo). The MADOCA and the AU/NZ SBAS products and their impacts on the POD of small LEO satellites with limited data were investigated in Allahvirdi-Zadeh et al. (2020).

However, even with high-precision real-time orbit and clock corrections available in space, some limitations should be considered for the onboard POD. For instance, most LEO satellites, especially those used for remote sensing applications, are in highly inclined polar orbits, which limits their ability to receive real-time GPS orbits and clock parameters via GEO satellites when the LEO satellite is over the polar region. The concept of using multi-antennas has been proposed by Giordano et al. (2017) to overcome the weak communication links above this region. Moreover, sudden communication breaks could result in discontinuities in receiving the required orbit and clock offset corrections. In such cases, using outdated corrections is inevitable. An alternative solution is predicting the orbit and clock corrections with, e.g., high-order polynomials (El-Mowafy et al. 2017). It was reported in Hauschild et al. (2016) that the predicted corrections improve the real-time POD of SWARMC satellite compared to the case when using broadcast ephemeris. The real-time orbit and clock corrections could also

contain faults or significant errors, which decrease their accuracy. To solve this problem, the orbits and clocks may be modeled as additional quasi-observations and be checked independently from the observations in an FDE (El-Mowafy 2018). Moreover, switching from one GEO satellite transmitter to other providers could also cause problems, as different providers may apply different models and initial values in the orbit and clock correction production.

Real-time POD of Small LEO Satellites and LEO mega-constellations

Recent low-cost GNSS receivers will be used in the future to test real-time POD in the low-power CubeSats (Palomo et al. 2019). Real-time POD is also essential for the LEO augmentation systems, which can be used to aid positioning in challenging areas with low GNSS visibility and to improve the PPP convergence time for ground users (Li et al. 2019). The generating procedure of the required orbital products for LEO constellations are proposed by Wang and El-Mowafy (2020). In addition to the orbits, prediction of the LEO clocks is also essential for positioning applications using LEO constellations. The clock prediction is affected by different factors such as the stability of the onboard frequency oscillator and the time reference, as well as the estimation errors and residuals in the POD procedure. The relevant factors and their potential influences were discussed and analysed by Wang and El-Mowafy (2021) for certain LEO clock types.

Based on the altitude of the LEO region, covering the whole Earth using a mega-constellation of large and expensive LEO satellites requires a huge budget. The available constellations of the small communication LEO satellites such as OneWeb (2021) and Starlink (2021) can be used to improve the positioning coverage and performance for urban areas, and possibility indoor, applications and intelligent transportation systems by providing additional positioning signals if supplied by navigation payloads (Reid et al. 2019), or with their signals used as signal-of-opportunity (Psiaki, 2020). However, the onboard POD is a challenging task, especially for the low-power satellites. Other information, such as inter-satellite links, could be used to strengthen the model. This approach has been tested by Li et al. (2019) for different simulated LEO satellite constellations using simulated inter-satellite links. The sub-cm to decimetres accuracies achieved in this method depends on the number of links and their ranging accuracies. The other issue in the constellation of the small LEO satellites, especially for the low-cost CubeSats, is the stability of the onboard frequency oscillator which is essential for the clock modelling of these satellites. Unstable oscillators prevent clock prediction and epoch-by-epoch clock estimation is required in the real-time POD procedure that should be performed either onboard or by the ground user.

Real-time POD with Integer Ambiguity Resolution

Although the POD based on IAR improves orbital accuracy in post-mission, performing the actual onboard POD with IAR is a challenging task and requires real-time phase corrections in space. As an example, the QZSS satellites broadcast these phase biases over Japan via the L6 signal (IS-QZSS-L6-003 2020) under the Centimetre Level Augmentation Service (CLAS). With the availability of such phase corrections in space, the onboard POD of the LEO satellites with PPP-IAR and its impacts on actual onboard POD can be tested in the near future.

Summary and Conclusion

In this paper, two main LEO POD methods, the kinematic and the reduced-dynamic POD, in two processing modes, the post-mission and the real-time processing, are reviewed and discussed. The kinematic POD uses only GNSS measurements and it is appropriate for the applications such as gravity missions that do not consider the dynamic forces affecting the LEO satellites. On the other hand, the reduced-dynamic POD is a more accurate method, as the dynamic models and estimated empirical accelerations can strengthen the measurement model and thus improve POD accuracy. In the post-processing mode, both the kinematic and the reduced-dynamic POD methods provide accurate orbits at several centimeters, fulfilling the required accuracy for most LEO missions. For example, gravity missions require kinematic orbits with an accuracy of a few centimeters. Other applications such as

altimetry, atmospheric sounding, and InSAR also use high-accuracy reduced-dynamic orbits, from one to several centimeter levels.

The numerical integration in the reduced-dynamic POD requires high computational efforts. Consequently, the reduced-dynamic POD is more time-consuming than the kinematic POD. With the powerful computation units in the processing centers available, the computational load is not a significant factor for post-processing and even the near-real-time applications. However, it has a considerable impact on the onboard processing since there could be not enough computational capacity in space, in particular for small LEO satellites such as CubeSats.

The kinematic POD is not available in the epochs experiencing data gaps, which is common for small LEO satellites with power limitations, such as CubeSats, as power sometimes has to be rotationally allocated among different sensors onboard. For these satellites, the reduced-dynamic POD is the proper method; however, simplified dynamic models can be considered to facilitate onboard POD. The reduced-dynamic POD is also the primary method for the reference orbit determination of LEO satellites in the orbit determination centers such as CODE and JPL.

Besides reviewing the post-mission procedures, the recent advancement in the onboard POD, such as using real-time precise orbits and clock corrections in space and its limitations in terms of availability, accuracy, continuity, and reliability, are addressed. The onboard POD is based on using filtering approaches. In applying comprehensive dynamic models and precise satellite orbits and clock corrections, the final output of the EKF after solution convergence can reach a similar level as that using the batch least-squares in the post-processing mode. However, due to the onboard processing limitations, simplified dynamic models are often used in the real-time POD, resulting in a degraded accuracy compared to the post-mission processing mode. Table 3 provides a comparison between the kinematic and the reduced-dynamic POD for both the post-mission and real-time modes.

Real-time POD and the corresponding challenges for the small low-capacity power satellites with limited data such as CubeSats are among our future works. The LEO POD enabled IAR, which has been tested in the post-processing mode, is considered as an appropriate tool for improving real-time POD performance. However, it requires real-time phase corrections in space for the onboard satellite positioning, which is currently limited and not tested yet in real-world LEO missions, but it is of high interest to the LEO community. The onboard POD is essential for formation flying of LEO satellites and LEO mega-constellations as a positioning augmentation system to GNSS. This is a new topic in navigation, remote sensing, and geoscience applications.

Data Availability Statement

All data, models, and code generated or used during the study appear in the submitted article.

Acknowledgments

The work is funded by the Australian Research Council Discovery Project: Tracking Formation-Flying of Nanosatellites Using Inter-Satellite Links (DP 190102444), and the Chinese Academy of Sciences (CAS) “Light of West China” Program (No. XAB2018YDYL01).

References

Allahverdi-Zadeh, A., J. Asgari, and A. R. Amiri-Simkooei. 2016. "Investigation of GPS draconitic year effect on GPS time series of eliminated eclipsing GPS satellite data." J. Geod. Sci. 6(1). https://doi.org/10.1515/jogs-2016-0007.

Allahvirdi-Zadeh, A., K. Wang, and El-Mowafy, A. 2021. "POD of small LEO satellites based on precise real-time MADOCA and SBAS-aided PPP corrections." GPS Solut. 25(31). https://doi.org/10.1007/s10291-020-01078-8.

Allahvirdi-Zadeh, A., K. Wang, and El-Mowafy, A. 2021. "Precise Orbit Determination of CubeSats Using Proposed Observations Weighting Model". In Proc. Geodesy for a Sustainable Earth, Scientific

Assembly of the International Association of Geodesy (IAG 2021). Beijing, China, https://files.sciconf.cn/upload/file/20210626/20210626085039_69146.pdf.

Altamimi, Z., P. Rebischung, L. Métivier, and X. Collilieux. 2016. "ITRF2014: A new release of the International Terrestrial Reference Frame modeling nonlinear station motions." J. Geophys. Res. Solid Earth 121(8): 6109-6131. https://doi.org/10.1002/2016JB013098.

Arnold, D., O. Montenbruck, S. Hackel, and K. Sośnica. 2019. "Satellite laser ranging to low Earth orbiters: orbit and network validation." J. Geod. 93(11): 2315-2334. https://doi.org/10.1007/s00190-018-1140-4.

Auriol, A., and C. Tourain. 2010. "DORIS system: The new age." Adv. Space Res. 46(12): 1484-1496. https://doi.org/10.1016/j.asr.2010.05.015.

Baarda, W. 1968. A testing procedure for use in geodetic networks. Delft: Netherlands Geodetic Commission.

Barrios, J., J. Caro, J. Calle, E. Carbonell, J. Pericacho, G. Fernández, V. Esteban, M. Fernández, F. Bravo, and B. Torres. 2018. "Update on Australia and New Zealand DFMC SBAS and PPP System Results." In Proc. of ION GNSS+ 2018, 1038-1067. https://doi.org/10.33012/2018.15932.

Bertiger, W., S. D. Desai, B. Haines, N. Harvey, A. W. Moore, S. Owen, and J. P. Weiss. 2010. "Single receiver phase ambiguity resolution with GPS data." J. Geod. 84(5): 327-337. https://doi.org/10.1007/s00190-010-0371-9.

Bertiger, W., Y. Bar-Sever, A. Dorsey, B. Haines, N. Harvey, D. Hemberger, M. Heflin, W. Lu, M. Miller, and A. W. Moore. 2020. "GipsyX/RTGx, A New Tool Set for Space Geodetic Operations and Research." Adv. Space Res. 66: 469–489. https://doi.org/10.1016/j.asr.2020.04.015.

Bock, H., A. Jäggi, U. Meyer, P. Visser, J. van den Ijssel, T. van Helleputte, M. Heinze, and U. Hugentobler. 2011. "GPS-derived orbits for the GOCE satellite." J. Geod. 85(11): 807. https://doi.org/10.1007/s00190-011-0484-9.

Bock, H., A. Jäggi, G. Beutler, and U. Meyer. 2014. "GOCE: precise orbit determination for the entire mission." J. Geod. 88(11): 1047-1060. https://doi.org/10.1007/s00190-014-0742-8.

Butcher, J. C. a. 2016. Numerical methods for ordinary differential equations. Chichester, West Sussex, England: John Wiley & Sons, Ltd.

Chuang, S., Z. Qile, G. Jianghui, L. Yidong, G. Maorong, and L. Jingnan. 2008. "Recent development of PANDA software in GNSS data processing." In Proc., International Conference on Earth Observation Data Processing and Analysis (ICEODPA), https://doi.org/10.1117/12.816261.

Dach, R., S. Lutz, P. Walser, and P. Fridez. 2015. Bernese GNSS Software Version 5.2. University of Bern: Bern Open Publishing.

El-Mowafy, A. 2014. "GNSS multi-frequency receiver single-satellite measurement validation method." GPS Solut. 18(4): 553-561. https://doi.org/10.1007/s10291-013-0352-6.

El-Mowafy, A., M. Deo, and N. Kubo. 2017. "Maintaining real-time precise point positioning during outages of orbit and clock corrections." GPS Solut. 21(3): 937-947. https://doi.org/10.1007/s10291-016-0583-4.

El-Mowafy, A. 2018. "Real-Time Precise Point Positioning Using Orbit and Clock Corrections as Quasi-Observations for Improved Detection of Faults." J. Navig. 71(4): 769-787. https://doi.org/10.1017/S0373463317001023.

Feng, Y., and Y. Zheng. 2005. "Efficient interpolations to GPS orbits for precise wide area applications." GPS Solut. 9(4): 273-282. https://doi.org/10.1007/s10291-005-0133-y.

Fernández, J., C. Fernández, P. Féménias, and H. Peter. 2016. "The Copernicus Sentinel-3 mission."ILRS Workshop. https://cddis.nasa.gov/lw20/docs/2016/papers/P32-Fernandez_paper.pdf.

Fernández, J., H. Peter, J. Berzosa, L. J. Gallardo, E. J. Calero, and P. Féménias. 2018. "Copernicus POD Service: First orbit determination results for Sentinel-3B."ESA reports: https://sentinel.esa.int/documents/247904/3372613/25-years-progress-radar-altimetry-first-orbit-determination-results-sentinel-3b.

Fernández, M. 2019. "Sentinel-3 Properties for GPS POD, Copernicus Sentinel-1, -2 and -3 Precise Orbit Determination Service. https://sentinels.copernicus.eu/documents/247904/3372613/Sentinel-3-GPS-POD-Properties.pdf.

Gerlach, C., N. Sneeuw, P. Visser, and D. Švehla. 2003. "CHAMP Gravity Field Recovery with the Energy Balance Approach: First Results." First CHAMP Mission Results for Gravity, Magnetic and Atmospheric Studies, C. Reigber, H. Lühr, and P. Schwintzer, eds., Springer Berlin Heidelberg, Berlin, Heidelberg, 134-139.

Giordano, P., P. Zoccarato, M. Otten, and M. Crisci. 2017. "P2OD: Real-time Precise Onboard Orbit Determination for LEO Satellites." In Proc. of the 30th International Technical Meeting of the Satellite Division of The Institute of Navigation (ION GNSS+ 2017), 1754-1771. https://doi.org/10.33012/2017.15190.

Giorgi G. 2017. "Attitude Determination." Springer Handbook of Global Navigation Satellite Systems, P. J. G. Teunissen, and O. Montenbruck, eds., Springer International Publishing, Cham, 561-582.

Guo, J., Q. Zhao, X. Guo, X. Liu, J. Liu, and Q. Zhou. 2015. "Quality assessment of onboard GPS receiver and its combination with DORIS and SLR for Haiyang 2A precise orbit determination." Sci. China Earth Sci. 58(1): 138-150. https://doi.org/10.1007/s11430-014-4943-z.

Haines, B., Y. Bar-Sever, W. Bertiger, S. Desai, and P. Willis. 2004. "One-Centimeter Orbit Determination for Jason-1: New GPS-Based Strategies." Mar. Geodesy 27(1-2): 299-318. https://doi.org/10.1080/01490410490465300.

Hauschild, A., O. Montenbruck, and P. Steigenberger. 2013. "Short-term analysis of GNSS clocks." GPS Solut. 17(3): 295-307. https://doi.org/10.1007/s10291-012-0278-4.

Hauschild, A., J. Tegedor, O. Montenbruck, H. Visser, and M. Markgraf. 2016. "Precise onboard orbit determination for LEO satellites with real-time orbit and clock corrections." In Proc. of the 29th International Technical Meeting of The Satellite Division of the Institute of Navigation (ION GNSS 2016), 3715-3723. https://doi.org/10.33012/2016.14717.

Hauschild, A., and O. Montenbruck. 2020. "Precise On-Board Navigation of LEO Satellites with GNSS Broadcast Ephemerides." In Proc. of the 33rd International Technical Meeting of the Satellite Division of The Institute of Navigation (ION GNSS+ 2020), 3866-3874. https://doi.org/10.33012/2020.17752.

Hofmann-Wellenhof, B., H. Lichtenegger, and E. Wasle. 2008. GNSS — Global Navigation Satellite Systems: GPS, GLONASS, Galileo, and more. Vienna: Vienna: Springer Vienna.

Hoque, M. M., and N. Jakowski. 2007. "Higher order ionospheric effects in precise GNSS positioning." J. Geod. 81(4): 259-268. https://doi.org/10.1007/s00190-006-0106-0.

Humpherys, J., and J. West. 2010. "Kalman Filtering with Newton's Method [Lecture Notes]." IEEE Control Syst. Mag. 30(6): 101-106. https://doi.org/10.1109/MCS.2010.938485.

IS-QZSS-L6-003 2020. "Quasi-Zenith Satellite System Interface Specification Centimeter Level Augmentation Service." Japanese Cabinet Office. https://qzss.go.jp/en/technical/download/pdf/ps-is-qzss/is-qzss-l6-003.pdf?t=1606870849719.

Jacchia, L. G. 1971. "Revised Static Models of the Thermosphere and Exosphere with Empirical Temperature Profiles." SAO Special Report.

Jäggi, A., G. Beutler, and U. Hugentobler. 2005. "Efficient Stochastic Orbit Modeling Techniques using Least Squares Estimators." In Proc., A Window on the Future of Geodesy, 175-180. Springer Berlin Heidelberg, https://doi.org/10.1007/3-540-27432-4_31.

Jäggi, A., U. Hugentobler, and G. Beutler. 2006. "Pseudo-Stochastic Orbit Modeling Techniques for Low-Earth Orbiters." J. Geod. 80(1): 47-60. https://doi.org/10.1007/s00190-006-0029-9.

Jäggi, A., U. Hugentobler, H. Bock, and G. Beutler. 2007. "Precise orbit determination for GRACE using undifferenced or doubly differenced GPS data." Adv. Space Res. 39(10): 1612-1619. https://doi.org/10.1016/j.asr.2007.03.012.

Jäggi, A., R. Dach, O. Montenbruck, U. Hugentobler, H. Bock, and G. Beutler. 2009. "Phase center modeling for LEO GPS receiver antennas and its impact on precise orbit determination." J. Geod. 83(12): 1145. https://doi.org/10.1007/s00190-009-0333-2.

Jäggi, A., C. Dahle, D. Arnold, H. Bock, U. Meyer, G. Beutler, and J. van Den Ijssel. 2016. "Swarm kinematic orbits and gravity fields from 18months of GPS data." Adv. Space Res. 57(1): 218-233. https://doi.org/10.1016/j.asr.2015.10.035.

Jokinen, A., C. Ellum, J. Neumann, D. Chan, I. Webster, S. Masterson, and T. Morley. 2014. "Kinematic performance of NovAtel CORRECT with terrastar-D Precise Point Positioning (PPP) service." In Proc. of the 27th International Technical Meeting of the Satellite Division of the Institute of Navigation (ION GNSS'14), 1020-1034.

Kang, Z., P. Nagel, and R. Pastor. 2003. "Precise orbit determination for GRACE." Adv. Space Res. 31(8): 1875-1881. https://doi.org/10.1016/S0273-1177(03)00159-5.

Kang, Z., S. Bettadpur, P. Nagel, H. Save, S. Poole, and N. Pie. 2020. "GRACE-FO precise orbit determination and gravity recovery." J. Geod. 94(9): 85. https://doi.org/10.1007/s00190-020-01414-3.

Kintner, P. M., B. M. Ledvina, and E. R. de Paula. 2007. "GPS and ionospheric scintillations." Space Weather. 5(9). https://doi.org/10.1029/2006SW000260.

Laurichesse, D., F. Mercier, J. P. Berthias, P. Broca, and L. Cerri. 2009. "Integer Ambiguity Resolution on Undifferenced GPS Phase Measurements and Its Application to PPP and Satellite Precise Orbit Determination." Navigation 56(2): 135-149. https://doi.org/10.1002/j.2161-4296.2009.tb01750.x.

Li, K., X. Zhou, W. Wang, Y. Gao, G. Zhao, E. Tao, and K. Xu. 2018. "Centimeter-Level Orbit Determination for TG02 Spacelab Using Onboard GNSS Data." Sensors 18(8): 2671. https://doi.org/10.3390/s18082671.

Li, M., W. Li, C. Shi, K. Jiang, X. Guo, X. Dai, X. Meng, Z. Yang, G. Yang, and M. Liao. 2017. "Precise orbit determination of the Fengyun-3C satellite using onboard GPS and BDS observations." J. Geod. 91(11): 1313-1327. https://doi.org/10.1007/s00190-017-1027-9.

Li, X., Z. Jiang, F. Ma, H. Lv, Y. Yuan, and X. Li. 2019. "LEO Precise Orbit Determination with Inter-satellite Links." Remote Sens. 11(18). https://doi.org/10.3390/rs11182117.

Li, X., F. Ma, X. Li, H. Lv, L. Bian, Z. Jiang, and X. Zhang. 2019. "LEO constellation-augmented multi-GNSS for rapid PPP convergence." 93(5): 749-764. https://doi.org/10.1007/s00190-018-1195-2.

Luzum, B. J., J. R. Ray, M. S. Carter, and F. J. Josties. 2001. "Recent Improvements to IERS Bulletin A Combination and Prediction." GPS Solut. 4(3): 34-40. https://doi.org/10.1007/PL00012853.

Ma, C., E. F. Arias, T. M. Eubanks, A. L. Fey, A. M. Gontier, C. S. Jacobs, O. J. Sovers, B. A. Archinal, and P. Charlot. 1998. "The international celestial reference frame as realized by very long baseline interferometry." Astron. J. 116(1): 516-546. https://doi.org/10.1086/300408.

Montenbruck, O., and E. Gill. 2000. Satellite Orbits: Models, Methods and Applications. Berlin, Heidelberg: Springer.

Montenbruck, O., T. van Helleputte, R. Kroes, and E. Gill. 2005. "Reduced dynamic orbit determination using GPS code and carrier measurements." Aerosp Sci Technol 9(3): 261-271. https://doi.org/10.1016/j.ast.2005.01.003.

Montenbruck, O., M. Markgraf, J. Naudet, S. Santandrea, K. Gantois, and P. Vuilleumier. 2008. "Autonomous and Precise Navigation of the Proba-2 Spacecraft." AIAA/AAS Astrodynamics Specialist Conference and Exhibit, American Institute of Aeronautics and Astronautics. https://doi.org/10.2514/6.2008-7086.

Montenbruck, O., and P. Ramos-Bosch. 2008. "Precision real-time navigation of LEO satellites using global positioning system measurements." GPS Solut. 12(3): 187-198. https://doi.org/10.1007/s10291-007-0080-x.

Montenbruck, O., M. Garcia-Fernandez, Y. Yoon, S. Schön, and A. Jäggi. 2009. "Antenna phase center calibration for precise positioning of LEO satellites." GPS Solut. 13(1): 23-34. https://doi.org/10.1007/s10291-008-0094-z.

Montenbruck, O. 2017. "Space Applications." Handbook of Global Navigation Satellite Systems, P. J. G. Teunissen, and O. Montenbruck, eds., Springer, Cham, 933-964.

Montenbruck, O., S. Hackel, and A. Jäggi. 2018. "Precise orbit determination of the Sentinel-3A altimetry satellite using ambiguity-fixed GPS carrier phase observations." J. Geod. 92(7): 711-726. https://doi.org/10.1007/s00190-017-1090-2.

Odijk, D., B. Zhang, A. Khodabandeh, R. Odolinski, and P. J. G. Teunissen. 2016. "On the estimability of parameters in undifferenced, uncombined GNSS network and PPP-RTK user models by means of S-system theory." J Geod. 90(1): 15-44. https://doi.org/10.1007/s00190-015-0854-9.

OneWeb. 2021" Accessed 1 June 2021. https://www.oneweb.world/.

Palomo, J. M., P. D'Angelo, P. F. Silva, A. J. Fernández, P. Giordano, P. Zoccarato, J. Tegedor, O. Oerpen, L. B. Hansen, C. Hill, and T. Moore. 2019. "Space GNSS receiver performance results with precise real-time on-board orbit determination (P2OD) in LEO missions." In Proc. of the 32nd International Technical Meeting of the Satellite Division of The Institute of Navigation (ION GNSS+ 2019), 1172-1186. https://doi.org/10.33012/2019.17082.

Pardal, P., H. Kuga, and R. V. de Morales. 2010. "Comparing the extended and the sigma point Kalman filters for orbit determination modeling using GPS measurements." In Proc. of the 23rd International Technical Meeting of the Satellite Division of The Institute of Navigation (ION GNSS 2010), 2732-2742.

Pavlis, N., S. Kenyon, J. Factor, and S. Holmes. 2008. "Earth gravitational model 2008." SEG Technical Program Expanded Abstracts 2008, Society of Exploration Geophysicists, 761-763.

Peter, H., A. Jäggi, J. Fernández, D. Escobar, F. Ayuga, D. Arnold, M. Wermuth, S. Hackel, M. Otten, W. Simons, P. Visser, U. Hugentobler, and P. Féménias. 2017. "Sentinel-1A – First precise orbit determination results." Adv. Space Res. 60(5): 879-892. https://doi.org/10.1016/j.asr.2017.05.034.

Petit, G., and B. Luzum. 2010. "IERS conventions." Verlag des Bundesamts für Kartographie und Geodäsie, (IERS Technical Note; 36) Frankfurt am Main. https://www.iers.org/IERS/EN/Publications/TechnicalNotes/tn36.html.

Psiaki, M. L. 2020. "Navigation using Carrier Doppler Shift from a LEO Constellation: TRANSIT on Steroids." In Proc. of the 33rd International Technical Meeting of the Satellite Division of The Institute of Navigation (ION GNSS+ 2020), September 2020, 3027-3045. https://doi.org/10.33012/2020.17667.

Reid, T., K. Gunning, A. Perkins, L. O. Sherman, and T. Walter. 2019. "Going back for the future: Large/MeGA LEO constellations for navigation." 2452-2468. https://doi.org/10.33012/2019.17123.

Ren, L., and S. Schön. 2018. "PPP-based Swarm kinematic orbit determination." Ann. Geophys. 36(5): 1227-1241. https://doi.org/10.5194/angeo-36-1227-2018.

Rothacher, M., and R. Schmid 2010. "ANTEX: The antenna exchange format version 1.4." Format specification, IGS Central Bureau, Pasadena (ftp://igs.org/pub/station/general/antex14.txt).

Standish, E. 1998. "JPL planetary and lunar ephemerides, DE405/LE405, JPL IOM 312." F-98_048.

Starlink Constellation. 2021. Accessed 1 June 2021. https://www.starlink.com/.

Švehla, D., and M. Rothacher. 2004. "Formation Flying of LEO Satellites Using GPS." American Geophysical Union, Fall Meeting 2004, SF53A-0735. https://ui.adsabs.harvard.edu/abs/2004AGUFMSF53A0735S.

Švehla, D. 2018. Geometrical Theory of Satellite Orbits and Gravity Field. Online: Springer.

Švehla, D., and M. Rothacher. 2003a. "Kinematic and reduced-dynamic precise orbit determination of low earth orbiters." Adv Geosci 1: 47-56. https://doi.org/10.5194/adgeo-1-47-2003.

Švehla, D., and M. Rothacher. 2003b. "CHAMP Double-Difference Kinematic POD with Ambiguity Resolution." First CHAMP Mission Results for Gravity, Magnetic and Atmospheric Studies, C. Reigber, H. Lühr, and P. Schwintzer, eds., Springer Berlin Heidelberg, Berlin, Heidelberg, 70-77.

Švehla, D., and M. Rothacher. 2005a. "Kinematic positioning of LEO and GPS satellites and IGS stations on the ground." Adv. Space Res. 36(3): 376-381. https://doi.org/10.1016/j.asr.2005.04.066.

Švehla, D., and M. Rothacher. 2005b. "Kinematic Precise Orbit Determination for Gravity Field Determination." In Proc., A Window on the Future of Geodesy, 181-188. Springer Berlin Heidelberg, https://doi.org/10.1007/3-540-27432-4_32.

Tegedor, J., O. Ørpen, T. Melgard, D. Lapucha, and H. Visser. 2017. "G4 Multi-constellation Precise Point Positioning Service for High Accuracy Offshore Navigation." TransNav 11(3): 425-429. https://doi.org/10.12716/1001.11.03.05.

Teunissen, P. J. G., and A. Khodabandeh. 2015. "Review and principles of PPP-RTK methods." J. Geod. 89(3): 217-240. https://doi.org/10.1007/s00190-014-0771-3.

Vallado, D. A., and D. Finkleman. 2014. "A critical assessment of satellite drag and atmospheric density modeling." Acta Astronaut. 95: 141-165. https://doi.org/10.1016/j.actaastro.2013.10.005.

Van Den Ijssel, J., J. Encarnação, E. Doornbos, and P. Visser. 2015. "Precise science orbits for the Swarm satellite constellation." Adv. Space Res. 56(6): 1042-1055. https://doi.org/10.1016/j.asr.2015.06.002.

Van den Ijssel, J., B. Forte, and O. Montenbruck. 2016. "Impact of Swarm GPS receiver updates on POD performance." Earth Planets Space 68(1): 85. https://doi.org/10.1186/s40623-016-0459-4.

Wang, K., A. Allahvirdi-Zadeh, A. El-Mowafy, and J. N. Gross. 2020. "A Sensitivity Study of POD Using Dual-Frequency GPS for CubeSats Data Limitation and Resources." Remote Sens. 12(13):2107. https://doi.org/10.3390/rs12132107.

Wang, K., and A. El-Mowafy. 2020. "Proposed Orbital Products for Positioning Using Mega-Constellation LEO Satellites." Sensors 20(20): 5806. https://doi.org/10.3390/s20205806.

Wang, K., and A. El-Mowafy. 2021. "LEO satellite clock analysis and prediction for positioning applications." Geo Spat Inf Sci: 1-20. https://doi.org/10.1080/10095020.2021.1917310.

Wang, L., R. Chen, D. Li, G. Zhang, X. Shen, B. Yu, C. Wu, S. Xie, P. Zhang, and M. Li. 2018. "Initial assessment of the LEO based navigation signal augmentation system from Luojia-1A satellite." Sensors 18(11): 3919. https://doi.org/10.3390/s18113919.

Weinbach, U., and S. Schön. 2012. "Improved GPS receiver clock modeling for kinematic orbit determination of the GRACE satellites." In Proc., 2012 European Frequency and Time Forum, 157-160. https://doi.org/10.1109/EFTF.2012.6502356.

Wermuth, M., O. Montenbruck, and T. Van Helleputte. 2010. "GPS high precision orbit determination software tools (GHOST)." In Proc., 4th international conference on astrodynamics tools and techniques, Madrid, Spain, 3-6. Citeseer, https://doi.org/10.1117/12.816261.

Xiong, C., H. Lühr, M. Schmidt, M. Bloßfeld, and S. Rudenko. 2018. "An empirical model of the thermospheric mass density derived from CHAMP satellite." In Proc., Annales Geophysicae, 1141-1152. Copernicus GmbH, https://doi.org/10.5194/angeo-36-1141-2018.

Yang, Y., X. Yue, J. Yuan, and C. Rizos. 2014. "Enhancing the kinematic precise orbit determination of low earth orbiters using GPS receiver clock modelling." Adv. Space Res. 54(9): 1901-1912. https://doi.org/10.1016/j.asr.2014.07.016.

Yang, Y., X. Yue, and A. G. Dempster. 2016. "GPS-based onboard real-time orbit determination for leo satellites using consider Kalman filter." 52(2): 769-777. https://doi.org/10.1109/TAES.2015.140758.

Yunck, T. P., W. I. Bertiger, S. C. Wu, Y. E. Bar-Sever, E. J. Christensen, B. J. Haines, S. M. Lichten, R. J. Muellerschoen, Y. Vigue, and P. Willis. 1994. "First assessment of GPS-based reduced dynamic orbit determination on TOPEX/Poseidon." Geophys. Res. Lett. 21: 541. https://doi.org/10.1029/94gl00010.

Zehentner, N., and T. Mayer-Gürr. 2016. "Precise orbit determination based on raw GPS measurements." J. Geod. 90(3): 275-286. https://doi.org/10.1007/s00190-015-0872-7.

Zhang, Q., X. Guo, L. Qu, and Q. Zhao. 2018. "Precise Orbit Determination of FY-3C with Calibration of Orbit Biases in BeiDou GEO Satellites." Remote Sens. 10(3): 382. https://doi.org/10.3390/rs10030382.

Tables

Table 1. Examples of dynamic models used in the reduced-dynamic POD.

Item	**Description**
Earth's gravity	EGM 2008 (Pavlis et al. 2008)
Tides (Solid Earth tides, Pole tides, and Ocean tides)	IERS 2010 (Petit and Luzum 2010)
Other planets ephemeris	JPL Development Ephemeris (JPL DE405) (Standish 1998)
Radiation pressure	Cannon-ball model (Montenbruck and Gill 2000), conical Earth shadow (Allahverdi-Zadeh et al. 2016)
Atmospheric drag	Jacchia 71 density model (Jacchia 1971)
	Daily solar flux and hourly geomagnetic activity (Xiong et al. 2018)
Antenna offset	Constant phase center coordinate in the SRF (Rothacher et al. 2010)
	Attitude information of the satellite (Giorgi 2017)
Empirical acceleration	Pseudo-stochastic pulses, Piecewise constant/continuous accelerations (Jäggi et al. 2006)
Terrestrial reference frame	ITRF2014 (Altamimi et al. 2016)
Earth orientation	IAU precession, nutation, and sidereal time models (Petit and Luzum 2010) - IERS polar bulletin (Luzum et al. 2001)
Inertial reference frame	ICRF (J2000.0) (Ma et al. 1998)

Table 2. Summary of LEO POD results in different studies (Acronyms are defined at the bottom)

Mission	**Accuracy in terms of RMS w.r.t. the reference solution (cm)**	**POD**	**Reference**
CHAMP	SLR RMS: 2.7	Kin[1]	(Švehla and Rothacher 2005b)
	SLR RMS: 2.5	RD[2]	
GRACE-A	SLR RMS: 2.2	RD	(Jäggi et al. 2007)
	SLR RMS: 3.0	Kin	
GRACE-B	SLR RMS: 1.9	RD	
	SLR RMS: 2.8	Kin	
GRACE	K-Band RMS: 1.1	RD	
	K-Band RMS: 2.0	Kin	
GOCE	SLR RMS: 2.3	Kin	(Bock et al. 2011)
	SLR RMS: 2.0	RD	
Swarm	SLR RMS: 4-5	Kin	(Van Den Ijssel et al. 2015)
	SLR RMS: 2	RD	
Swarm-A	SLR RMS: 3.2	Kin	(Jäggi et al. 2016)
Swarm-B	SLR RMS: 2.7		
Swarm-C	SLR RMS: 3.1		
Fengyun-3C	Overlapping 3D RMS: 3.4	RD	(Li et al. 2017)
TG02	Overlapping 3D RMS: 1.4 SLR RMS < 3.5	RD	(Li et al. 2018)

Sentinel 1-A	QWG 3D RMS[3] < 2.5	RD	(Peter et al. 2017, Fernández et al. 2018, Fernández 2019)
Sentinel 1-B	QWG 3D RMS < 4		
Sentinel 2-A	QWG 3D RMS < 2.5		
Sentinel 2-B	QWG 3D RMS < 2		
Sentinel 3-A	QWG 3D RMS < 3 SLR RMS < 1.5		
Sentinel 3-B	QWG 3D RMS < 3 SLR RMS < 1.5		
GRACE-FO C	SLR RMS: 1.5	RD	(Kang et al. 2020)
GRACE-FO D	SLR RMS: 1.5		
GRACE-FO	K-Band RMS: 0.5		

[1]Kin: Kinematic, 2 RD: Reduced-dynamic, [3] QWG: QWG 3D RMS values were achieved by comparing Copernicus POD solutions with the POD Quality Working Group as external solutions.

Table 3. Comparison of the POD methods that are typically used in the post-processing and real-time modes.

	Post-mission POD		**Real-time POD**	
	Kinematic	**Reduced-dynamic**	**Kinematic**	**Reduced-dynamic**
Inputs	GNSS observation, GNSS satellite orbits and clock corrections	Dynamic models, GNSS observations + GNSS satellite orbits and clock corrections	GNSS observation, broadcast ephemeris	Simplified dynamic models, GNSS observation, broadcast ephemeris
Outputs	Satellite positions, LEO receiver clock offsets, phase ambiguities	Keplerian elements (initial state), force model parameters, empirical accelerations, LEO receiver clock offsets, phase ambiguities	Satellite positions, LEO receiver clock offsets, phase ambiguities	Keplerian elements (initial state), force model parameters, empirical accelerations, LEO receiver clock offsets, phase ambiguities
Limitations	Data problems and gaps	Model deficiencies	Data problems and gaps	Computational load
Advantages	Computational effectiveness, not relying on dynamic models	High accuracy and continuity	Computational effectiveness, not relying on dynamic models	High accuracy and continuity
Usability	Gravity missions	Most geoscience and remote sensing missions	Onboard positioning and navigation	Onboard positioning and navigation
Accuracy	< 10 cm	< 5 cm	Meter	Sub-meter

Figure Caption List

Fig. 1. Flowchart of the paper structure.

Fig. 2. Questions that will be addressed in each section.

Fig. 3. Flowchart of reduced-dynamic POD computation procedure.

Fig. 4. Flowchart for the EKF reduced-dynamic POD